Agricultural plastic waste spatial estimation by Landsat8 satellite images

Antonio Lanorte[a] , Fortunato De Santis[a], Gabriele Nolè[a], Ileana Blanco[b] , Rosa Viviana Loisi[b], Evelia Schettini[b*], Giuliano Vox[b]

[a] IMAA - CNR - C.da Santa Loja, zona industriale, Tito Scalo, 85050 Potenza, Italy

[b] University of Bari - Department of Agricultural and Environmental Science (DISAAT), via Amendola 165/A, 70126, Bari, Italy

[*] Corresponding author

Evelia Schettini

Tel: +39 080 5443547 - Fax: +39 080 5442977

Email: evelia.schettini@uniba.it

ORCID:

Blanco Ileana: 0000-0003-2927-3427

Loisi Rosa Viviana: 0000-0003-3618-5118

Schettini Evelia: 0000-0002-8456-8677

Vox Giuliano: 0000-0003-4017-5174

Agricultural plastic waste spatial estimation by Landsat8 satellite images

Antonio Lanorte[a] , Fortunato De Santis[a], Gabriele Nolè[a], Ileana Blanco[b] , Rosa Viviana Loisi[b], Evelia Schettini[b*], Giuliano Vox[b]

[a] IMAA - CNR - C.da Santa Loja, zona industriale, Tito Scalo, 85050 Potenza, Italy

[b] University of Bari - Department of Agricultural and Environmental Science (DISAAT), via Amendola 165/A, 70126, Bari, Italy

[*] Corresponding author

Abstract

The use of plastic materials in agriculture involves several benefits but it results in huge quantities of agricultural plastic waste to be disposed of. Input and output data on the use of plastics in agriculture are often difficult to obtain and poor waste management schemes have been developed. The present research aims to estimate and map agricultural plastic waste by using satellite images. Waste was evaluated by means of the indexes relating waste production to crop type and plastic application as defined by the land use map realized by classifying the Landsat8 image. The image classification was carried out using the Support Vector Machines (SVMs), the accuracy assessment showed that the overall accuracy was 94.54% and the Kappa coefficient equal to 0.934. Data on the plastic waste obtained by the satellite land use map were compared with the data obtained by using the institutional land use map; a difference of 1.75 % was pointed out on the overall quantity of waste.

Keywords: agricultural plastic waste; waste generation; waste collection; remote sensing; land conservation

1. Introduction

Plastics are nowadays indispensable in modern agriculture, they are used for crop protection and shading, soil mulching, irrigation pipes, silage covering, harvesting and post-harvesting operations, pots, trays and seedling containers, packaging containers and sacks (Markarian, 2005; Vox et al., 2010; Picuno, 2014).

The use of plastic materials in agriculture, known as plasticulture, involve benefits in terms of light weight and good mechanical resistance, easy installation, use and management, lower cost in relation to other materials. Plastic covering films and nets protect crop from adverse weather conditions and from birds and aphids, extend the harvest season and improve crop quality and yield by realizing favourable growing climatic conditions for the plants. Plastic films for soil mulching decrease the use of chemicals for weed control, reduce water consumption and preserve plants and edible products both from the soil diseases and from the dirt, thus improving the plants health and the yield quality (Briassoulis and Schettini, 2003; Mistriotis and Castellano, 2012; Picuno et al., 2012; Briassoulis et al., 2013). All these properties explain the widespread use of plastics in agriculture that are mainly based on low density polyethylene (LDPE), ethylene vinyl acetate (EVA), high density polyethylene (HDPE), polypropylene (PP), polyvinyl chloride (PVC) (Markarian, 2005; Castellano et al., 2008; Hopewell et al., 2009; Scarascia-Mugnozza et al., 2011; Briassoulis et al., 2013; Simboli et al., 2015).

The yearly consumption of agricultural plastics in the world amounts to 6.5 million tons that result in huge quantities of Agricultural Plastic Waste (APW) to be disposed of by reason of the frequent substitution of the plastic products.

The sustainable management on the land of APW is part of the wider issue of the land conservation (Picuno et al. , 2011; Díaz-Palacios-Sisternes et al., 2014, Vox et al., 2016a, Scarascia-Mugnozza et al., 2016).

At the end of their useful life, only a small percentage of APW is recycled: in EU the amount of agricultural plastic materials used in 2011 was more than 1.3 million tonnes, the recovery rate of agricultural plastics has been only 46% and the mechanical recycling rate has been about 23% (PasticsEurope, 2013; González-Sánchez et al., 2014).

Unlike in urban areas APW in rural land must be collected over wide areas and so it requires a suitable system of waste management in order to optimize the localization of the first collection centres. Poor and inefficient APW management schemes have been developed in Europe so far, input and output data on the use of plastics in agriculture are often difficult to obtain (Briassoulis *et al.*, 2013). APW is seasonally dependent, so its quantity varies both with the time and with the localization depending on the crop type. Plastic waste must be estimated every few months in order to optimize the collection procedure. One way to estimate APW on the land is to use information about the cultivated crop; land use maps realized by institutions can be used for this purpose but unfortunately they are often updated with a low temporal resolution and lack information on the presence of plastic covering (film or nets) for crop protection (Sica et al., 2015; Scarascia-Mugnozza et al., 2016; Vox et al., 2016b). Satellite images with a higher temporal resolution can be used in order to estimate APW, the Landsat satellites, for example, cross every point on Earth once every 16 days.

Remote sensing of plastic coverings is a particular field of application of the automatic mapping techniques of land use due to several peculiarities; it strongly depends on the spatial, temporal and spectral characteristics of the considered objects and of the sensor due to: the similarity of plastic agricultural equipments with other buildings, the plastics spectral signal changing with the

underlying vegetation reflectance properties; the seasonally dependent use of plastic covering films (Levin et al., 2007; Aguilar et al., 2014; Loisi et al., 2015).

Automated object recognition from remote sensing images, compared to manual digitizing, saves time and avoids the use of skilled technicians delegated to visual recognition. It can be carried out according to two different analysis approaches: the pixel-based approach and the object-based approach. These analysis approaches aim to define a biunivocal relation between the pixels constituting an image and the classes of information set as goal of the detection. The pixel-based approach operates on single pixels and takes into account only their spectral characteristics. The object-based approach focuses on regions, on objects made of several pixels that correspond the objects on the site; the object-based approach takes into account both spectral and spatial data. The pixel-based image analysis employs the unsupervised and the supervised learning techniques. The unsupervised technique, also called image clustering, requires the pixels to be firstly classified in groupings according to numerical information by means of clustering algorithms; then to be associated to information classes by an operator. The supervised technique instead requires that the information classes are defined previously by the operator which identifies a certain number of Areas Of Interest (AOI) in an image, i.e. the training sites. The AOI are used in order to elaborate the spectral signature of each information class. The whole of all the spectral signatures are the basis on which suitable algorithms operate for detecting areas in the image having spectral similarities with the AOI. The object-based approach is based on the use of specific algorithms that carry on the image classification according to two different methods: the recognition of pixel-intensity discontinuity, the recognition of pixel-intensity similarity (Arcidiacono et al., 2010a; Weih and Riggan, 2010; Duro et al., 2012).

Low-Medium resolution satellite data, such as MODIS (low) and Landsat (medium) images that are free online available data, are characterized by a large pixel size and large ground sample distance (GSD). The recent availability of very high-resolution (VHR) data, provided by

commercial satellites such as IKONOS and QuickBird, and then of better performing satellites such as GeoEye-1 (GE-1) and WorldView-2 (WV-2), has led to further developments in the urban and rural planning sector (Levin et al., 2007; Tarantino and Figorito, 2012; Aguilar et al., 2014; Novelli and Tarantino, 2015). VHR data have proved to be very suitable for plastic coverings mapping, nevertheless also Landsat images can be useful in detecting plastic coverings depending on the area size of the studied objects (Levin et al., 2007; Novelli and Tarantino, 2015) and even in identifying the greenhouse horticultural crops (Aguilar et al., 2015).

Levin et al. (2007) found good results in detecting plastic coverings in agricultural landscapes by means of the hyperspectral technology. Using AISA-ES, an airborne imaging spectrometer, which provides hyperspectral data, they achieved a detection accuracy of above 90% for bright sheets and nets and of only 70% for the black nets from an AISA-ES image having a spatial resolution of 1m.

Arcidiacono and Porto (2010b) compared the object-based image analysis (OBIA) technique and the pixel-based analysis, both supervised and unsupervised, in detecting crop-shelter coverage by aerial RGB digital images; they assessed that the object-oriented method reduced the computational time and produced more detailed results. Arcidiacono and Porto (2010a) proposed a model to manage crop-shelter spatial development by means of automatic image analyses based on OBIA technique, geographical information system (GIS) processing and the definition of Driving force-Pressure-State-Impact-Response spatial indicators.

Tarantino and Figorito (2012) applied the OBIA to Very High Spatial Resolution true colour aerial data, with a GSD of 0.20 m, in order to detect land use and to map in detail vineyards plastic coverings on eight test areas. The classes detected were bare soil, orchard, vegetables, plastic sheet vineyard, hail net vineyard and uncovered vineyard. A preliminary segmentation process was applied to the images; the classification process was carried on exploiting the Feature Space Optimization (FSO), an algorithm applied in eCognition software, to define optimal combination of features to improve the classification performance by selecting the set of features that produces the

best class separable distances (Chutia et al., 2014). The output result is the mapping of areas with prevalent plastic covered vineyards directly in polygonal form and with an overall accuracy of 90.25%.

Tasdemir and Koc-San (2014) applied an unsupervised learning approach to plastic and glass greenhouses extraction. They used WV-2 images in order to extract the spectral properties of the greenhouses using the image bands and their spatial characteristics using Gabor textural features. The two series of features were merged and clustered by an approximate spectral clustering based on local density similarity. The resulting overall accuracy was 87.30% and the kappa coefficient was 0.81, which were obtained with limited input data provided by the user.

Aguilar et al. (2014) exploited 3D information from VHR stereo pairs satellite images in order to better delineate objects with relevant height. They compared the greenhouse classification from GE-1 and WV-2 by using data sets constituted by spectral information from panchromatic and pan-sharpened multiangle orthoimages and single-source stereo-photogrammetrically derived heights; they applied an OBIA approach, using the non-parametric supervised nearest neighbor classifier, and reached similar overall accuracies from GE-1 and WW-2 tests.

In order to test the usefulness of medium-resolution sensor data, Picuno et al. (2011) carried out an analysis on the use of land by means of crops protected with plastics using Landsat images. The analysis was developed with the application of a supervised parallelepiped classification to multitemporal Landsat TM images, image processing, vectorialization and GIS utilities; it led to the generation of multi-temporal thematic maps areas covered with plastic films and to the possibility of creating a routine in IDL and ENVI software for automatically detecting the plastic coverings.

Landsat-8 Operational Land Imager (OLI) and Thermal Infrared Sensor (TIRS) data suitability for plasticulture detection were also successfully tested by means of four normalized difference indices, namely the green Normalized Difference Vegetation Index, the rescaled brightness temperature, the Plastic Surface Index and the Normalized Difference Sandy Index (Novelli and

169 Tarantino, 2015). The resulting maximum overall accuracy was higher than 80%, the joint use of
170 such indexes enhanced the contrast between the studied object and the other.

171 MODIS time series proved to be useful data to be analyzed with a threshold model, a one-class
172 classification method, for the detection of plastic-mulched land-cover on large geographic areas; the
173 resulting maps were found equivalent to maps produced using Landsat ETM+ and OLI images and
174 the maximum likelihood classification (MLC) method (Lu et al., 2015).

175 The Support Vector Machines (SVMs) are supervised automatic algorithms based on machine
176 learning theory (Zhu and Blumberg, 2002). They are non parametric classifiers that have a great
177 ability in optimizing classification issues, through the minimization of the empirical classification
178 errors and the maximization of the class separations (Nolè et al., 2015). Koc-San (2013) compared
179 the performance of random forests, maximum likelihood and SVM classifiers for glass greenhouse
180 and plastic greenhouse detection using WV-2 data. The greenhouses were identified from WV-2
181 satellite imagery with high overall accuracy for three methods, but the highest overall accuracy
182 resulted from SVM (93.88%), followed by the random forests one (91.73%).

183 Huang et al. (2002) detected land cover applying the SVM classification to spatially degraded
184 Landsat Thematic Mapper (TM) data; the application of the maximum likelihood algorithm and of
185 the decision tree algorithm generated a lower level of accuracy. The SVM classification technique
186 has been applied to a tropical coastal zone and has been compared with the MLC and Artificial
187 Neural Network techniques; the SVM algorithm performed better in separating human
188 infrastructures with spectral signatures similar to natural landscape components (Szuster et al.,
189 2011). The SVM gave better results in terms of accuracy in comparison to MLC when applied to
190 ASTER imagery of the northwestern India for the automated lithological classification (Yu et al.,
191 2012). Yousefi et al. (2011) carried out a comprehensive study on the comparison of the nine
192 supervised classification algorithms (SVM, Neural network, Mahalanobis distance, Maximum
193 likelihood, Minimum distance, Spectral angle mapper, Spectral information divergence,

parallelepiped and binary code) as tools for land use mapping starting from Landsat ETM+ images; they asserted the superiority of the SVM algorithm which showed the best results, that is a kappa coefficient of 0.9503 and an overall accuracy of 90.94 %. Several studies report on the application of the SVM algorithm for pattern recognition: greater accuracy has been achieved by SVM in comparison to MLC and artificial neural network (NN) (Deilmai et al., 2014).

The present paper proposes a method for identifying, localizing and quantifying APW, based on the application of the SVM classification technique to OLI images. The aim is to study the convenience of using free online available satellite data in evaluating APW by comparing them with the waste data obtained from less frequent higher resolution maps. The method was tested in the Apulia Region (Southern Italy), over an area characterized by a widespread use of the "tendone" technique that is a traditional grape cultivation system; this technique is realized with a supporting structure that may be covered with plastic film or net so generating huge quantities of plastic wastes (Picuno et al., 2011; Vox et al., 2012; Sica et al., 2015).

2. **Study area**

The study area is located in the Apulia Region, Southern Italy, between the municipalities of Noicattaro and Mola di Bari (Fig. 1); the area, which has an extension of 15 km^2 (3x5 km), is centered on the WGS84 geographic coordinates of 41.046°N and 17.029 ° E (WGS 84 UTM: zone 33 N, 670550 E, 4545870 N).

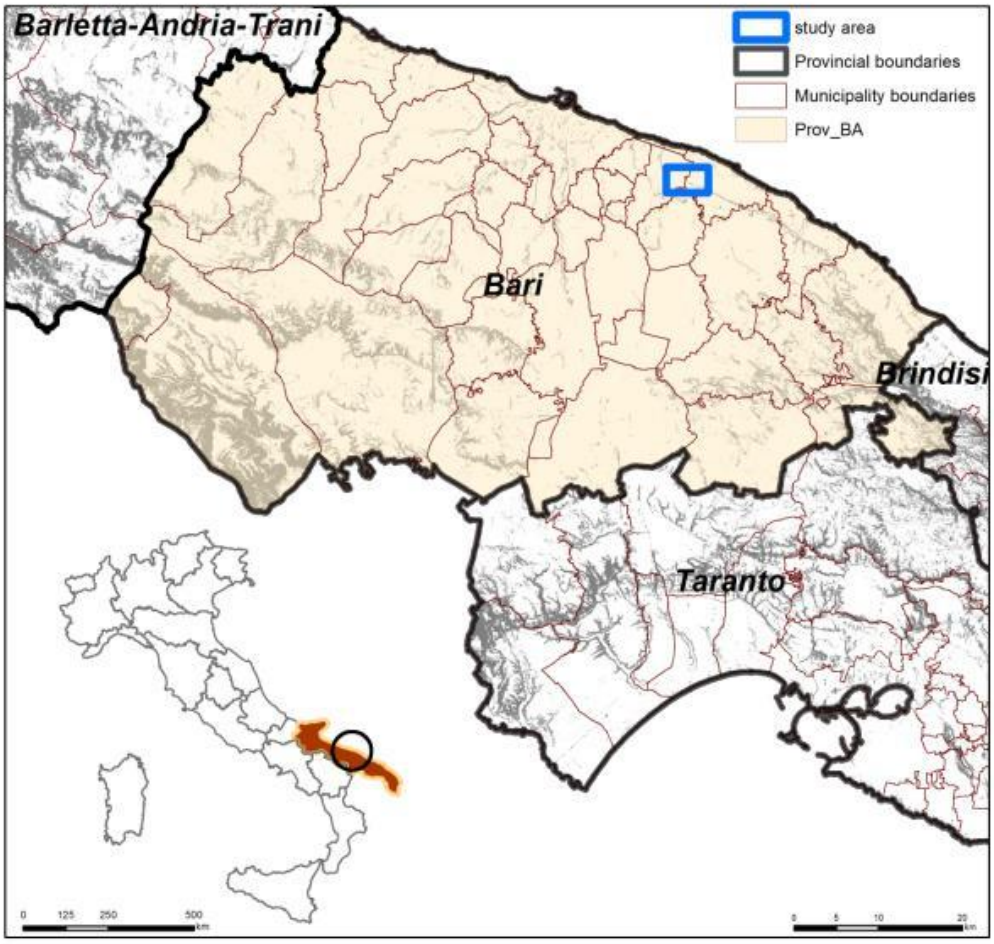

Figure 1: The study area located in Southern Italy.

The area is characterised by intensive agriculture and huge quantities of APW dealing with several applications are generated: irrigation pipes, agro-chemicals containers, bags for fertilizers, films for mulching and films and nets for crop protection. A huge amount of waste is originated from films and nets as the agriculture is mainly dedicated to table grape cultivation protected with plastic film or net. Plastic films are generally mounted over the crop from February to July in order to advance the harvesting or from August to December to delay it; nets are mounted in the same periods, but they are often kept mounted throughout the year. Plastic films are made with LDPE or EVA, nets mostly with HDPE.

3. Methodology

Two methods for the evaluation of APW in the land were used: one was based on the land use map available on the Apulia region website, the other one on the land use map obtained from the satellite image. Both the maps were related to the indexes quantifying plastic waste generation for each crop type and plastic application in order to obtain the waste quantities on the land. The results obtained with the two methodologies were compared.

3.1 Waste evaluation from the Regional map

The crop type was evaluated by means of the land use map of the Apulia Region, realized in 2006 and updated in 2011, at a scale of 1:5,000: it derives from an orthophoto having 50 cm pixel; the legend complies with the European CORINE Land Cover Changes Database with an extension to the fourth level. The map is available on the website of the Apulia Region (http://www.sit.puglia.it) and can be downloaded in the different shape files associated to the different portions of the territory forming the study area. The different shape files were merged in order to have a unique shape file that was subjected to a clip operation on the study area; the shape file was placed in the WGS 84 / UTM zone 33N reference system.

241

Table 1: Plastic Waste Index (PWI) per Crop Type (CT) and Plastic Application (PA)

CT	PA	PWI (kg ha^{-1} yr^{-1})
vineyard	plastic film	613.80
	anti-hail net	159.03
	irrigation pipe	83.33
	fertilizer bag	1.60
	agrochemicals container	4.00
olive grove	irrigation pipe	50.00
	fertilizer bag	0.50
	agrochemicals container	0.63
orchard	irrigation pipe	62.50
	fertilizer bag	2.20
	agrochemicals container	1.80
vegetable	irrigation pipe	69.44
	fertilizer bag	2.50
	agrochemical container	1.70

242

243 The following plastic wastes were considered: irrigation pipes, agro-chemicals containers, bags
244 for fertilizers, films and nets for crop protection.

245 The regional land use map provides information on the spatial distribution of the different crops
246 (vineyard, olive grove etc.), but the information about the presence and the type of the vineyards
247 protection, i.e. net or film, is missing because it is an information highly variable on a monthly

basis. The data on the presence of plastic films and nets were obtained by the photo-interpretation of an image dated May 18, 2013 provided by the web-mapping tool Google Maps. Thence the corrected land use map was produced and the APW on the land was calculated on the basis of the crop type and of the indexes shown in table 1 that estimate the waste generation for each crop type and plastic application; the indexes were obtained by means of questionnaire delivered to several growers of the area (AWARD project, 2016).

The waste for each Plastic Application (PA) of the i-th parcel, which is characterized by its Crop Type (CT), was calculated by:

(1)

where S_i is the surface of the i-th parcel, $PWI_{CT,PA}$ is the plastic waste index for the CT of the i-th parcel and for the specific PA.

The total waste for each i-th parcel, including all the applications, was calculated by:

(2)

where N is the number of PAs for the crop type present in the i-th parcel.

3.2 Waste evaluation from the satellite image

The application of a system with a higher temporal resolution for evaluating APW was carried out by means of satellite data.

Satellite image interpretation could be difficult in some areas especially in presence of covering plastic film or net; in order to have a clear basis for the definition of the spectral fingerprints and the subsequent creation of a suitable training set for the satellite image interpretation, two specific shape files were created, based on the above mentioned regional map; each shape file included 10 sample areas regarding vineyards covered with nets and vineyard covered with plastic film,

respectively. After the definition of the spectral fingerprints a land use map, based on the satellite data, was created. Finally, the values of the APW were calculated by means of the indexes that estimate the plastic waste generation for each crop type and plastic application as above described for the regional map; in this case the parcel corresponds to the pixel of the satellite image.

3.2.1 **Data**

A Landsat8 OLI-TIRS image provided by the USGS EROS Center (USGS, 2015) was used; its acquisition date is May 19, 2013 (Fig. 2). The OLI and TIRS are sensors onboard the Landsat 8 satellite, which was launched in February 2013. Landsat8 collects images with a 16-day repeat cycle in a repetitive, near polar, sun-synchronous and circular orbit at 705 km of altitude.

The OLI sensor includes 9 spectral bands (table 2) with a spatial resolution of 30 m for Band 1 to Band 7 and Band 9. The resolution for Band 8 (panchromatic) is 15 m. Compared to previous Landsat mission (Landsat7) there are two new bands: band 1 (ultra-blue) is useful for coastal and aerosol studies and band 9 is useful for cirrus cloud detection.

The TIRS provides two thermal bands (bands 10 and 11) useful in providing more accurate surface temperatures which are collected at 100 meters but resampled to 30 meter in delivered data product.

Landsat8 images provide improved signal-to-noise (SNR) radiometric performance quantized over a 12-bit dynamic range. This translates into 4096 potential grey levels in an image compared with only 256 grey levels in previous 8-bit instruments. Improved signal to noise performance enable better characterization of land cover state and condition. Products are delivered as 16-bit images (scaled to 55,000 grey levels).

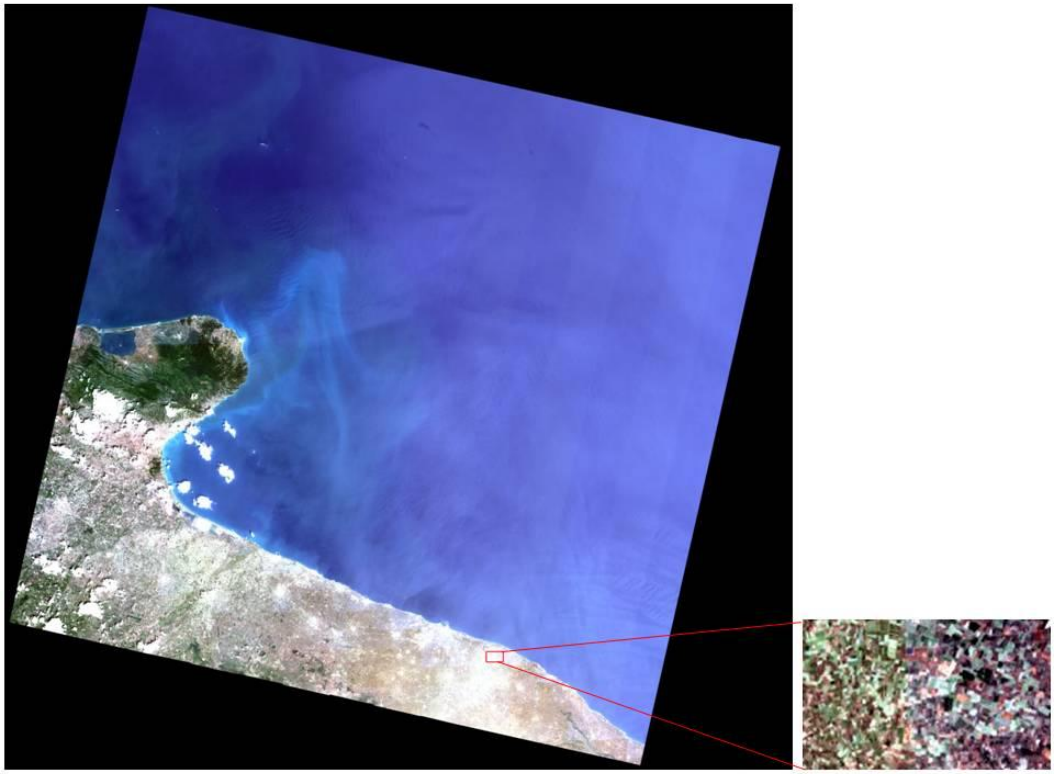

Figure 2: Landsat8 OLI-TIRS image (May 19, 2013) - RGB: 432. Red box: study area.

The study area is covered in scene path/row 188/31 with an approximate scene size of 170 km north-south by 183 km east-west.

The images were subjected to geometric, radiometric and atmospheric correction.

Standard Landsat8 data products consist of quantized and calibrated scaled Digital Numbers (DN) representing multispectral image data acquired by both the OLI and TIRS Sensors. The products are delivered in 16-bit unsigned integer format and were rescaled to the Top Of Atmosphere (TOA) reflectance and radiance using radiometric rescaling coefficients provided in the product metadata file (MTL file). The MTL file also contains the thermal constants needed to convert TIRS data to the at-satellite brightness temperature.

OLI and TIRS band data were converted to TOA spectral radiance using the following radiance rescaling factors provided in the metadata file:

$$L_\lambda = M_L Q_{cal} + A_L \quad (3)$$

where:

L_λ = TOA spectral radiance ($Wm^{-2}srad^{-1}\mu m^{-1}$)

M_L = Band-specific multiplicative rescaling factor from the metadata

(RADIANCE_MULT_BAND_x, where x is the band number)

A_L = Band-specific additive rescaling factor from the metadata (RADIANCE_ADD_BAND_x,

where x is the band number)

Q_{cal} = Quantized and calibrated standard product pixel values (DN)

The following equation is used to convert DN values to TOA reflectance for OLI data as follows:

$$\rho\lambda' = M_\rho Q_{cal} + A_\rho \quad (4)$$

where:

$\rho\lambda'$ = TOA planetary reflectance, without correction for solar angle.

M_ρ = Band-specific multiplicative rescaling factor from the metadata

(REFLECTANCE_MULT_BAND_x, where x is the band number)

A_ρ = Band-specific additive rescaling factor from the metadata (REFLECTANCE_ADD_BAND_x,

where x is the band number)

TOA reflectance with a correction for the sun angle is then:

$$\frac{\rho\lambda'}{\sin(\theta_{SE})} = \frac{\rho\lambda'}{\cos(\theta_{SZ})} \quad (5)$$

where:

$\rho\lambda$ = TOA planetary reflectance

θ_{SE} = Local sun elevation angle. The scene center sun elevation angle in degrees is provided in the

metadata (SUN_ELEVATION).

θ_{SZ} = Local solar zenith angle; $\theta_{SZ} = 90° - \theta_{SE}$

In this work we didn't use TIRS bands and, therefore, we didn't converted bands 10 and 11 from spectral radiance to brightness temperature.

Table 2: Landsat 8 Operational Land Imager (OLI) and Thermal Infrared Sensor (TIRS) - launched February 11, 2013

Band	Wavelength (μm)	Resolution (m)
Band 1 - Coastal aerosol	0.43 - 0.45	30
Band 2 - Blue	0.45 - 0.51	30
Band 3 - Green	0.53 - 0.59	30
Band 4 - Red	0.64 - 0.67	30
Band 5 - Near Infrared (NIR)	0.85 - 0.88	30
Band 6 - SWIR 1	1.57 - 1.65	30
Band 7 - SWIR 2	2.11 - 2.29	30
Band 8 - Panchromatic	0.50 - 0.68	15
Band 9 - Cirrus	1.36 - 1.38	30
Band 10 - Thermal Infrared (TIRS) 1	10.60 - 11.19	100 * (30)
Band 11 - Thermal Infrared (TIRS) 2	11.50 - 12.51	100 * (30)

3.2.2 Image Classification

The Landsat image was classified using the Support Vector Machines (SVMs), namely those supervised automatic algorithms based on machine learning theory (Zhu and Blumberg, 2002). SVMs are non parametric classifiers which proved very able at solving problems related to

343 classifications due to the ability of maximizing the class separations minimizing the classification
344 errors (Nolè et al., 2015); SVM algorithms and models use the supervised learning approach
345 (machine learning) for data analysis (Dixon and Candade, 2008).

346 We adopted SVMs in this study as this approach has shown remarkable potential for data
347 classification also in satellite data processing (Mountrakis et al., 2011).

348 According to Mountrakis et al. (2011), the use of SVM in remote sensing can successfully
349 manage small training data sets and perform better than other more traditional classifiers.

350 Like all non-parametric classifiers, also SVMs are used without the prior assumptions on the
351 probability distribution function of the data. This characteristic makes SVMs very suitable in
352 remote sensing applications since data acquired from remotely sensed imagery usually have
353 unknown distributions (Mountrakis et al., 2011).

354 Several studies demonstrated better performances of SVMs in terms of speed of training and
355 accuracy classification than other parametric and non-parametric classifiers (Mountrakis et al.,
356 2011).

357 SVM approaches, as for other supervised learning algorithms, require a training set, consisting of
358 m training samples made up of n vectors of input, named features X_i of m dimension and labels of
359 "correct answers" that we want the algorithm predicts.

360 In the case of satellite images, the training sets are pixels (identified as training samples)
361 described as vectors, whereas the labels are the given classes assigned for those pixels.

362 In this study we applied the SVM classification using ENVI 4.7 software (ITT, 2009; Wu et al.,
363 2004; Hsu et al., 2007). ENVI's implementation of SVM uses the pairwise classification strategy for
364 multiclass classification. SVM classification output is the decision values of each pixel for each
365 class, which are used for probability estimates. The probability values, stored in ENVI as rule
366 images, represent "true" probability in the sense that each probability falls in the range of 0 to 1, and

the sum of these values for each pixel equals 1. ENVI performs classification by selecting the highest probability.

Accuracy assessment

For the accuracy assessment we created the square contingency table matrix and evaluated the producer, user and overall accuracy and the k coefficient.

The producer accuracy is a measure indicating the probability that the classifier has correctly labeled an image pixel into Class A given that the ground truth is Class A. For example if the Class A has a total of *n* ground truth pixels where *m* pixels are classified correctly, the producer accuracy is the ratio *m*/*n*.

The user accuracy is a measure indicating the probability that a pixel is Class A given that the classifier has labelled the pixel into Class A. For example if the classifier has labeled *x* pixels as the Class A and a total of *y* pixels are classified correctly, the user accuracy is the ratio *y* / *x*.

Overall accuracy was computed as the sum of the number of observations correctly classified (class1, as class 1, class 2 as class 2, etc.) divided by the total number of observations. This is equivalent to the "diagonal" of the square contingency table matrix divided by the total number of observations described in that contingency table (Congalton and Green, 1998).

Kappa statistic measures the increase in classification accuracy over that of pure chance by accounting for omission and commission error (Congalton and Green, 1998).

4. Results and Discussion

The regional and the satellite land use map were the necessary basis for the following evaluation of the agricultural plastic waste on the land. The already available regional map was corrected in a few points by means of the photo-interpretation while the satellite land use map was built by means of the satellite image classification.

392

393 **4.1 The land use map from the satellite image**

394 On the basis of the land use map and the Google Earth high resolution image (Fig. 3), both
395 corresponding to the Landsat image acquisition period, we selected the region of interest (ROI)
396 corresponding to the land use classes.

397

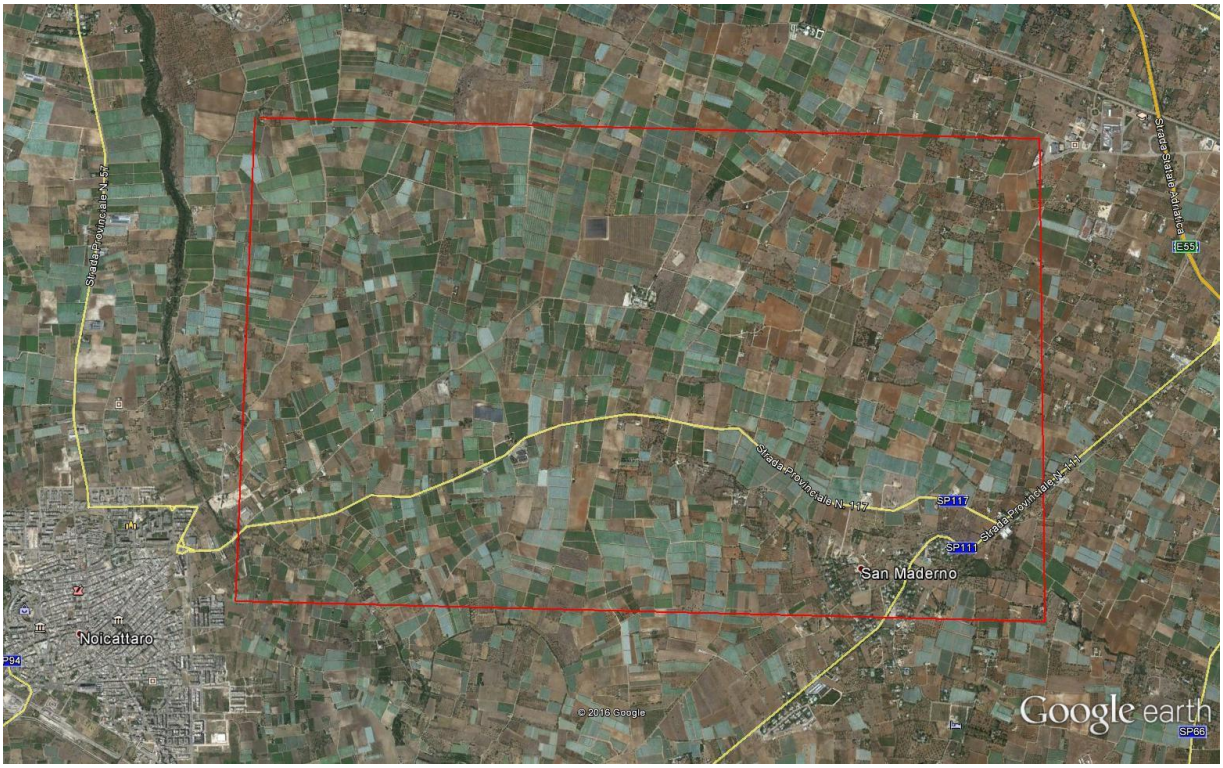

398

399

400 Figure 3: Google Earth high resolution image (May 18, 2013). Red box: study area.

401

402

403 Pixels belonging to each of the considered ROI were separated randomly into data training and
404 data testing, used for the SVM classification and accuracy evaluation, respectively.

405 Figure 4 shows the land use map obtained for the investigated test area from the Landsat image.
406 We reached the better results by using SVM classifiers with RBF kernel, Gamma=1 and Cost=1000
407 applied on 6 Landsat bands (2-7).
408

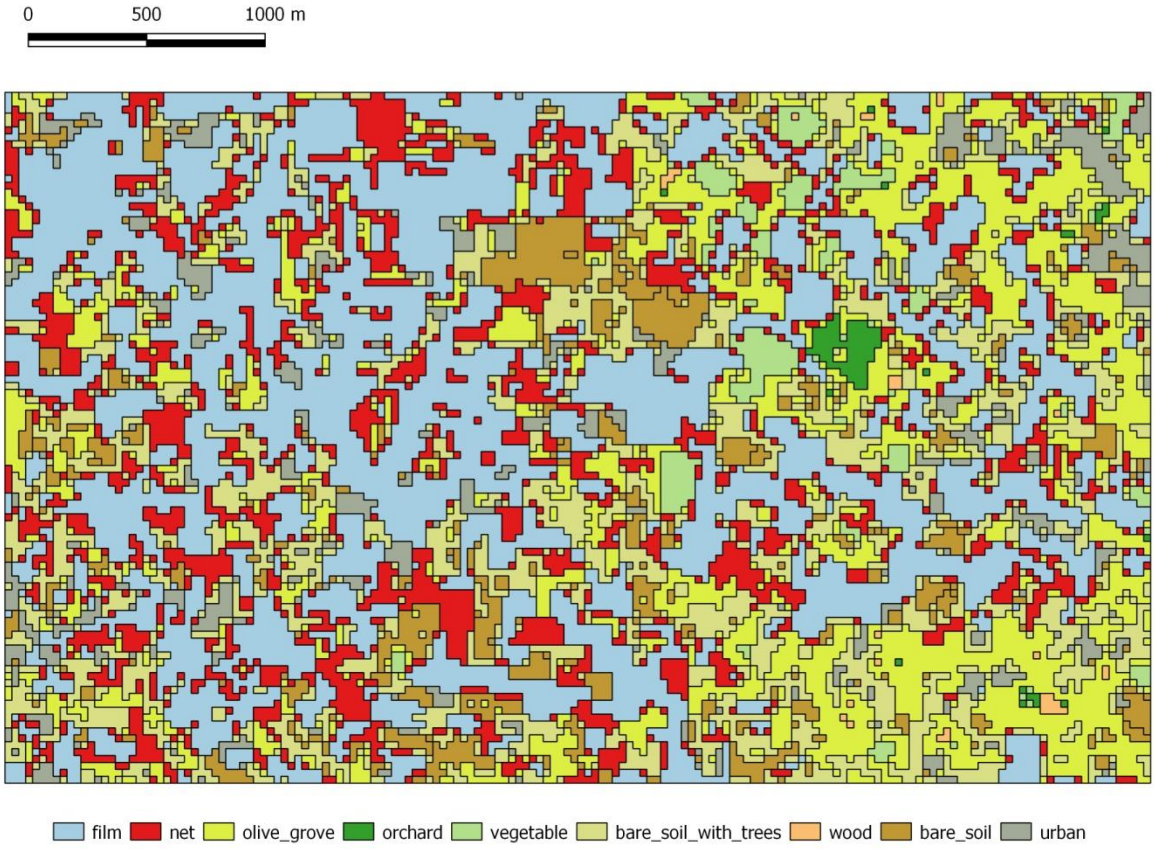

409
410 **Figure 4:** Land use map obtained from the Landsat8 image.
411
412 Such map presents very high accuracy levels that were assessed by means of the square
413 contingency table matrix (table 3) and by evaluating the producer, user and overall accuracy and the
414 kappa coefficient.
415

Table 3: Square contingency table matrix

	Ground Truth (%)									
Class		Film	Net	Bare soil	Vegetables	Orchards	Olive groves	Urban	Wood	Bare soil with trees
Film		**94.87**	2.38	0.00	0.00	0.00	0.00	7.14	0.00	7.14
Net		5.13	**97.62**	0.00	0.00	0.00	22.22	0.00	0.00	7.14
Bare soil		0.00	0.00	**100.00**	0.00	0.00	0.00	0.00	0.00	0.00
Vegetable		0.00	0.00	0.00	**100.00**	0.00	0.00	0.00	0.00	0.00
Orchard		0.00	0.00	0.00	0.00	**100.00**	0.00	0.00	0.00	0.00
Olive grove		0.00	0.00	0.00	0.00	0.00	**77.78**	0.00	0.00	7.14
Urban		0.00	0.00	0.00	0.00	0.00	0.00	**92.86**	0.00	0.00
Wood		0.00	0.00	0.00	0.00	0.00	0.00	0.00	**100.00**	0.00
Bare soil with trees		0.00	0.00	0.00	0.00	0.00	0.00	0.00	0.00	**78.57**
	Total	100.00	100.00	100.00	100.00	100.00	100.00	100.00	100.00	100.00

The *Film* class has an error of just over 5%, then about 5% of the total ground truth pixels of this class is not classified correctly; such pixels in this case are in the *Net* Class (Table 3).

Net class has an error of 2.38%. The pixels corresponding to this percentage in this case are in the *Film* Class (Table 3).

Worse results were pointed out for olive groves, 77.78% of the total ground truth pixels of this class were correctly classified.

425

Table 4: Producer and User Accuracies for each class		
Class	**Producer Acc. (%)**	**User Acc. (%)**
Film	94.87	96.10
Net	97.62	82.00
Bare soil	100.00	100.00
Vegetable	100.00	100.00
Orchard	100.00	100.00
Olive grove	77.78	93.33
Urban	92.86	100.00
Wood	100.00	100.00
Bare soil with trees	78.57	100.00

426

427

428 Table 4 shows the Producer and User Accuracies for each class.

429 The producer accuracy has the same values of the "diagonal" of the square contingency table
430 matrix.

431 The column of the User Accuracy indicates that the *Film* class has an error of less than 4%,
432 corresponding to the percentage of pixels that the classifier has labelled in *Film* class but actually
433 belong to other classes (*Net, Urban* and *Bare soil with trees*).

434 More significant is the mistake of the User Accuracy in *Net* class (18%). In this case then SVM
435 has labelled in *Net* class some pixels belonging to other classes, in particular to the *Film* class (8%),
436 *Olive Groves* class (8%) and *bare soil with trees* class (2 %).

437 The overall accuracy on the whole image was 94.54% with the Kappa coefficient equal to 0.934.

438

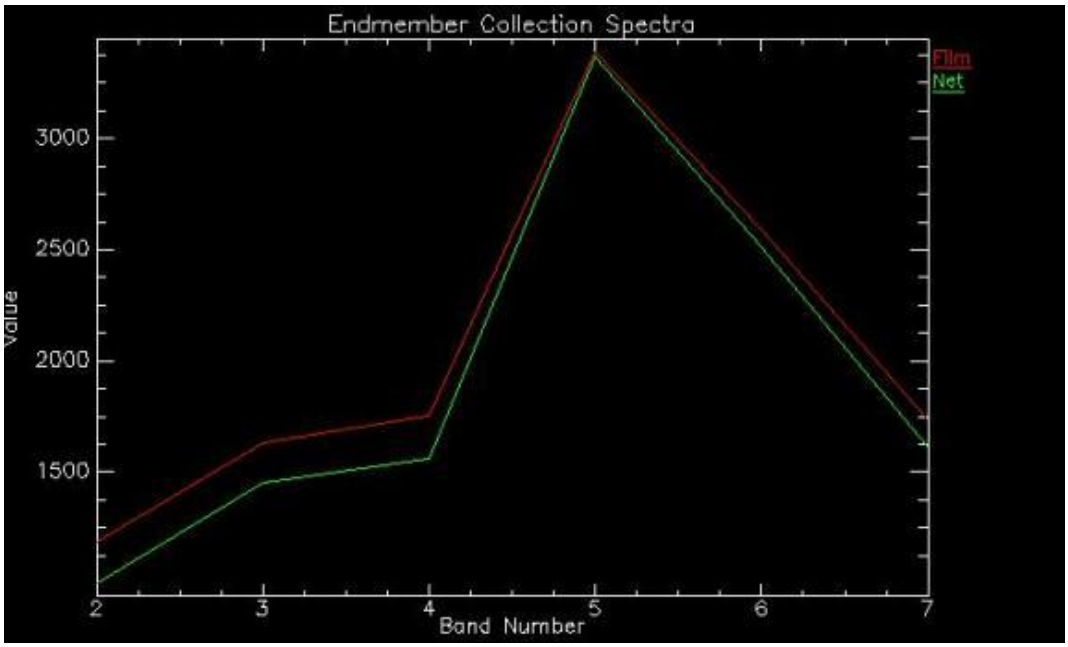

Figure 5: Spectral signatures of Film and Net.

Finally SVM showed high ability to detect the vineyards coverings (Films and Nets) with errors due to limited mixing between Film and Net classes and Net and Olive Groves classes.

The spectral signatures of Film and Net are shown in Figure 5. Also Jeffries-Matusita ROI separability test (Swain and Davis, 1978) showed value greater than 1.9 (1.971) for Film and Net and this demonstrated that the classes are well separated. In general Jeffries-Matusita test shows that all nine classes have significant spectral separability with each other.

Several authors have pointed out the higher classification accuracy generated by the Support Vector machines. Huang et al. (2002) implemented the SVM classification for a spatially degraded Landsat Thematic Mapper (TM) data. The SVM classification accuracy was superior to that obtained using a maximum likelihood algorithm and a decision tree algorithm. Yousefi et al. (2011) investigated the nine supervised classification algorithms (SVM, Neural network, Mahalanobis distance, Maximum likelihood, Minimum distance, Spectral angle mapper, Spectral information divergence, parallelepiped and binary code) in land use mapping in Mazandaran province, Iran and

used Landsat ETM+ images. Their results confirmed that the SVM classification, with a kappa coefficient of 0.9503 and an overall accuracy of 90.94 %, is better than the other methods. These results are compatible with those obtained in this study, demonstrating the reliability of SVM in land use mapping.

The findings obtained in the classification of films and nets, also confirm the reliability of SVM in identifying artificial elements. For example Szuster et al. (2011) examined the performance of the SVM classification technique in the tropical coastal zone and compared this technique with the MLC and Artificial Neural Network techniques, concluding that the SVM is better classifier for challenges like separating human infrastructures, for instance buildings from rocks and sandy beaches as they possess similar spectral signatures. In the case of our study we have a similar situation with two artificial objects (film and net) very close from spectral point of view. Also Koc-San (2013) has analyzed the accuracy of maximum likelihood, random forests and SVM classifiers for glass greenhouse and plastic greenhouse using WV-2 data. The results show that greenhouse can be identified from WV-2 imagery and all the accuracy for three methods are high, with the highest one from SVM, followed by random forests.

Finally, although this study did not provide a comparative analysis of the performance of SVM against other classifiers, with good approximation we can to affirm that the results obtained can be the best possible, in relation to the used sensor. To confirm this, we mentionYu et al. (2012) which have applied the support vector machine (SVM) algorithm for the automated lithological classification in a part of northwestern India using ASTER imagery. They have also showed that SVM gives higher accuracy in comparison to MLC. Furthermore the SVM algorithm has been used widely for pattern recognition applications and many researchers in this field have found that a higher level of accuracy can be achieved by SVM than other algorithm of classification like MLC (Oommen et al., 2008; Mondal et al., 2012), Artificial Neural Network (ANN) (Naguib et al., 2009), MLC and Artificial Neural Network (ANN) (Pal and Mather, 2005).

481

482 **4.2. The Agricultural Plastic Waste**

483 Both the regional map and the Landsat8 image map, together with the APW indexes (Tab.1),
484 were used to calculate the agricultural plastic waste on the land. Table 5 summarizes, for all the
485 parcels, the plastic waste as a function the crop type and of the plastic application. Given that data
486 obtained from the regional map (Regional base map in table 5) were assumed as true, the accuracy
487 of the waste evaluation with Landsat8 image (Landsta8 satellite base map in table 5) was affected
488 by the accuracy of land use classification carried out on the image.

489

Table 5: Plastic wastes as a function the crop type and of the plastic application.

Application	plastic films		anti-hail nets		irrigation pipes		fertilizer bags		agrochemicals containers		TOTAL	
Base map *	Reg.	Sat.	Reg.	Sat.	Reg.	Sat.	Reg.	Sat.	Reg.	Sat.	Reg.	Sat.
Crop type	(t)											
vineyard	341.89	322.01			46.42	43.72	0.89	0.84	2.23	2.10	391.43	368.66
vineyard with			28.15	34.88	14.75	18.28	0.28	0.35	0.71	0.88	43.89	54.39
vegetable					0.26	2.19	0.01	0.08	0.01	0.05	0.28	2.32
orchard					1.00	0.47	0.04	0.02	0.03	0.01	1.06	0.50
olive grove					9.73	12.65	0.10	0.13	0.12	0.16	9.95	12.94
Total	341.89	322.01	28.15	34.88	72.15	77.30	1.32	1.41	3.09	3.20	446.60	438.80
Error (t)		-19.89		6.73		5.15		0.10		0.11		-7.80
Error (%)		-5.82		23.92		7.14		7.28		3.51		-1.75

490

491 * : Reg.: regional; Sat.: Landsta8 satellite;

492

493

494 The highest value of plastic waste (341.9 tonnes), 76.6 % of the total APW (446.6 tonnes)
495 evaluated with the regional map, was pointed out for the films; the value evaluated by the satellite
496 map was 5.82 % lower than the value evaluated with the regional map, it corresponds to an error of
497 19.85 waste tonnes.
498 The error of detection of the plastic films is related to the low average size of the vineyard parcel
499 areas that are sometimes comparable or even smaller than the pixels size of the Landsat8 images.
500 The highest percentage error was recorded for the anti-hail nets even if anti-hail nets produced a
501 lower quantity of waste tonnes. The higher percentage error for the nets (23.92%) can be explained
502 with the difficulty of net detection caused by their low reflectivity due to the permeable structure.
503 The evaluation of the waste by the satellite map showed a good accuracy for the irrigation pipes, the
504 agro-chemical containers and the fertilizer bags, with a maximum percentage error of 7.28 %
505 recorded for the fertilizer bags.
506
507 **5. Conclusions**
508 Waste management is a global issue that should be addressed in a sustainable way. Agricultural
509 activities contribute to the generation of huge quantities of plastic wastes that must be correctly
510 disposed of. One of the problems is that input and output data on the use of plastics in agriculture
511 are often difficult to obtain; the proposed methodology uses satellite data for geo-referring
512 agricultural plastic wastes in this way obtaining updated waste maps. Waste managers can easily
513 use this information as basis of the waste management plan in order to define the position of the
514 collections centers and the waste route maps. The advantage of the use of free satellite images is
515 that they allow a high temporal resolution, comparable with the use of the plastic materials in the
516 agricultural activities. Support Vector Machines SVMs used for image classification showed high
517 ability to detect the different crops and the presence of plastic covering materials. The comparison
518 of the data on the waste generation obtained from satellite images with the data from the regional

519 map, verified and updated with photo-interpretation, highlighted the effectiveness of the
520 methodology.
521

522 **References**

523 Arcidiacono C., Porto S.M.C., 2010a. A model to manage crop-shelter spatial development by
524 multi-temporal coverage analysis and spatial indicators, Biosystems Engineering, 107 (2),
525 107-122.
526 Arcidiacono C., Porto S.M.C., 2010b. Classification of crop-shelter coverage by remote-sensing
527 images: a compendium of experiences and findings, Journal of agricultural engineering, 3, 1-
528 11.
529 Aguilar M. A., Bianconi F., Aguilar F. J., Fernández I., 2014. Object-Based Greenhouse
530 Classification from GeoEye-1 and WorldView-2 Stereo Imagery. Remote Sens., 6 (5), 3554-
531 3582.
532 Aguilar M. A., Vallario A., Aguilar F. J., Lorca A. G., Parente C., 2015. Object-Based Greenhouse
533 Horticultural Crop Identification from Multi-Temporal Satellite Imagery: A Case Study in
534 Almeria, Spain. Remote Sens., 7 (6), 7378-7401.
535 AWARD project, 2016. Agricultural Waste valorisation for a competitive and sustainable Regional
536 Development – AWARD project. European Territorial Cooperation Programme Greece-Italy
537 2007-13, contract n. I3.11.03. Collection Statistical Data from farmers, http://www.award-
538 project.eu/products/
539 Briassoulis D., Schettini E., 2003. Analysis and design of low-density polyethylene greenhouse
540 films. Biosystems Engineering 84 (3), 303-314. DOI: 10.1016/S1537-5110(02)00241-6.
541 Briassoulis D., Babou E., Hiskakis M., Scarascia G., Picuno P., Guarde D., Dejean C., 2013.
542 Review, mapping and analysis of the agricultural plastic waste generation and consolidation

in Europe. Waste Management & Research, 31 (12), 1262-1278. DOI: 10.1177/0734242X13507968.

Castellano, S.; Scarascia-Mugnozza, G.; Russo, G.; Briassoulis, D.; Mistriotis, A.; Hemming, S.; Waaijenberg, D., 2008. Plastic nets in agriculture: a general review of types and applications. Appl Eng Agric, 24 (6), 799-808.

Chutia D., Bhattacharyya D.K., Kalita R., Sudhakar S., 2014. OBCsvmFS: Object-Based Classification supported by Support Vector Machine Feature Selection approach for hyperspectral data. Journal of Geomatics, 8 (1), 12-19.

Congalton R.G., Green K., 1998. Assessing the accuracy of remotely sensed data. CRC Press, Lewis Publishers, Boca Raton, Florida, USA.

Deilmai B., Ahmad B., Zabihi H., 2014. Comparison of two classification methods (MLC and SVM) to extract land use and land cover in Johor Malaysia. IOP Conf. Ser. Earth Environ. Sci., 20, 1-6.

Díaz-Palacios-Sisternes, S. , Ayuga, F. , García, A.I., 2014. A method for detecting and describing land use transformations: AN examination of Madrid's southern urban-rural gradient between 1990 and 2006. Cities, 40, 99-110. DOI: 10.1016/j.cities.2014.03.010.

Dixon B., Candade N., 2008. Multispectral landuse classification using neural networks and support vector machines: one or the other, or both? Int. J. Remote Sens. 29 (4), 1185–1206.

Duro D. C, Franklin S. E., Dubé M.G., 2012. A comparison of pixel-based and object-based image analysis with selected machine learning algorithms for the classification of agricultural landscapes using SPOT-5 HRG imagery, Remote Sensing of Environment, 118, 259-272.

González-Sánchez C., Martínez-Aguirre A., Pérez-García B., Martínez-Urreaga J., U. de la Orden M., Fonseca-Valero C., 2014. Use of residual agricultural plastics and cellulose fibers for obtaining sustainable eco-composites prevents waste generation, Journal of Cleaner Production, 83, 228-237, ISSN 0959-6526, http://dx.doi.org/10.1016/j.jclepro.2014.07.061.

568 Hopewell J., Dvorak R., Kosior E., 2009. Plastics recycling: challenges and opportunities. Phil.
569 Trans. R. Soc. B 364, 2115–2126. DOI:10.1098/rstb.2008.0311.
570 Hsu, C.-W., Chang, C.-C., and Lin, C.-J., 2007. A practical guide to support vector classification.
571 National Taiwan University. http://ntu.csie.org/~cjlin/papers/guide/guide.pdf.
572 Huang C., Davis L.S., Townshend J.R.G., 2002. An assessment of support vector machines for land
573 cover classification. Int. J. Remote Sens, 23, 725-749.
574 ITT cooperation, 2009. ENVI 4.7 software. White Plains, NY.
575 Koc-San D., 2013. Evaluation of Different Classification Techniques for the Detection of Glass and
576 Plastic Greenhouses from WorldView-2 Satellite Imagery, Appl. Remote Sens, 7 (1), 1913-
577 1928.
578 Levin N., Lugassi R., Ramon U., Braun O., Ben-Dor E., 2007. Remote sensing as a tool for
579 monitoring plasticulture in agricultural landscapes, International Journal of Remote Sensing,
580 28 (1), 183-202.
581 Loisi R.V., Sica C., Blanco I., Schettini E., Scarascia Mugnozza G., Vox G., 2015. Land analysis of
582 agricultural plastic wastes production in a South Italy area by means of a Geographical
583 Information System, International Symposium on New Technologies and Management for
584 Greenhouses. GreenSys 2015. July 19-23 2015, Evora, Portugal. In: Acta Horticulturae (*in*
585 *press*).
586 Lu L., Hang D., Di L., 2015. Threshold model for detecting transparent plastic-mulched landcover
587 using moderate-resolution imaging spectroradiometer time series data: a case study in
588 southern Xinjiang, China", J. Appl. Remote Sens. 9 (1), 097094. DOI:
589 10.1117/1.JRS.9.097094.
590 Markarian J., 2005. Plasticulture comes of age, Plastics, Additives and Compounding, 7 (1), 16-19.
591 Mistriotis A., Castellano S., 2012. Airflow through net covered tunnel structures at high wind
592 speeds. Biosystems Engineering, 113 (3), 308-317.

593 Mondal A., Kundu S., Chandniha S. K., Shukla R., Mishra P., 2012. Comparison of Support Vector
594 Machine and Maximum Likelihood Classification Technique using Satellite Imagery.
595 International Journal of Remote Sensing and GIS, 1 (2), 116-123
596 Mountrakis G., Im J., Ogole C., 2011. Support vector machines in remote sensing: a review. ISPRS
597 J. Photogramm. 66 (3), 247–259.
598 Naguib A., Farag M., Yahia M., Ramadan H., Abd Elwahab M., 2009. Comparative study between
599 support vector machines and neural networks for lithological discrimination using
600 hyperspectral data. Egypt Journal of Remote Sensing and Space Science, 12, 27-42.
601 Nolè G., Murgante B., Calamita G., Lanorte A., R. Lasaponara, 2015. Evaluation of urban sprawl
602 from space using open source technologies. Ecological Informatics 26 (2), 151-161, ISSN
603 1574-9541. DOI: 10.1016/j.ecoinf.2014.05.005.
604 Novelli A., Tarantino E., 2015. Combining ad hoc spectral indices based on LANDSAT-8
605 OLI/TIRS sensor data for the detection of plastic cover vineyard, Remote Sensing Letters, 6
606 (12), 933-941. DOI: 10.1080/2150704X.2015.1093186.
607 Oommen T., Misra D., Twarakavi N. K., Prakash A., Sahoo B., Bandopadhyay S., 2008. An
608 objective analysis of support vector machine based classification for remote sensing.
609 Mathematical Geosciences, 40, 409-424.
610 Pal M., Mather P., 2005. Support vector machines for classification in remote sensing. International
611 journal of remote sensing, 26, 1007-1011.
612 Picuno P., Tortora A., Capobianco R. L., 2011. Analysis of plasticulture landscapes in Southern
613 Italy through remote sensing and solid modelling techniques. Landscape and Urban Planning,
614 100 (1-2), 45-56. DOI: 10.1016/j.landurbplan.2010.11.008.
615 Picuno P., Sica C., Laviano R., Dimitrijevic A., Scarascia-Mugnozza G., 2012. Experimental tests
616 and technical characteristics of regenerated films from agricultural plastics. Polymer
617 Degradation and Stability, 97 (9), 1654-1661.

618 Picuno P., 2014. Innovative Material and Improved Technical Design for a Sustainable Exploitation
619 of Agricultural Plastic Film Polymer. Plastics Technology and Engineering 53 (10), 1000-
620 1011.
621 PlasticsEurope, 2013. Plastics - the Facts 2012: An analysis of European plastics production,
622 demand and waste data for 2011.http://www.plasticseurope.org/Document/plastics-the-facts-
623 2012.aspx?FolID=2 (2012), January, 2013.
624 Scarascia-Mugnozza G., Sica C., Russo G., 2011. Plastic materials in European agriculture: actual
625 use and perspectives. Journal of Agricultural Engineering, 3, 15-28.
626 Scarascia-Mugnozza G., Schettini E., Loisi R.V., Blanco I., Vox G., 2016. Georeferencing of
627 agricultural plastic waste. Rivista di Studi sulla Sostenibilità, 2016 (1), 71-82. DOI:
628 10.3280/RISS2016-001007.
629 Sica C., Loisi R. V., Blanco I., Schettini E., Scarascia Mugnozza G., Vox G. (2015). Swot analysis
630 and land management of plastic wastes in agriculture. Actual Tasks on Agricultural
631 Engineering. Proc. 43rd International Symposium on Agricultural Engineering, 24-
632 27.02.2015, Opatija, Croatia, p. 745-754. ISSN 1848-4425. http://atae.agr.hr.
633 WOS:000373450700069.
634 Simboli A., Taddeo R., Morgante A., 2015. The potential of Industrial Ecology in agri-food clusters
635 (AFCs): A case study based on valorisation of auxiliary materials, Ecological Economics,
636 111, 65-75, ISSN 0921-8009. DOI: 10.1016/j.ecolecon.2015.01.005.
637 Swain, P. H., and S. M. Davis. 1978. Remote Sensing: The Quantitative Approach. New York:
638 McGraw Hill Book Company.
639 Szuster B. W., Chen Q., Borger M., 2011. A comparison of classification techniques to support land
640 cover and land use analysis in tropical coastal zones. Applied Geography, 31, 525-532, DOI:
641 10.1016/j.apgeog.2010.11.007.

642 Tarantino E., Figorito B., 2012. Mapping Rural Areas with Widespread Plastic Covered Vineyards
643 Using True Color Aerial Data. Remote Sensing, 4 (7), 1913-1928.
644 Tasdemir K., Koc-San D., 2014. Unsupervised extraction of greenhouses using WorldView-2
645 images, International Geoscience and Remote Sensing Symposium (IGARSS), art. no.
646 6947597, 4914-4917.
647 USGS, 2015. Landsat Missions, http://landsat.usgs.gov.
648 Vox G., Scarascia Mugnozza G, Schettini E., Tarricone L., Gentilesco G., De Palma L., Vitali M.,
649 2012. Radiometric properties of plastic films for vineyard covering and their influence on
650 vine physiology and production. Acta Horticulturae 956, 465-472.
651 Vox G., Teitel M., Pardossi A., Minuto A., Tinivella F., Schettini E., 2010. Chapter 1: Sustainable
652 Greenhouse Systems, in "Sustainable Agriculture: Technology, Planning and Management".
653 In: Salazar, A., Rios, I., eds., Nova Science Publishers, Inc. NY USA, 1-79.
654 Vox G, Maneta A and Schettini E., 2016a. Evaluation of the radiometric properties of roofing
655 materials for livestock buildings and their effect on the surface temperature. Biosystems
656 Engineering 144(April 2016): 26-37. DOI: 10.1016/j.biosystemseng.2016.01.016.
657 Vox G., Loisi R.V., Blanco I., Scarascia Mugnozza G., Schettini E., 2016b. Mapping of agriculture
658 plastic waste, Agriculture and Agricultural Science Procedia, 8: 583-591. DOI:
659 10.1016/j.aaspro.2016.02.080.
660 Weih R.C. Jr., Riggan N.D.Jr., 2010. Object-Based Classification vs. Pixel-Based Classification:
661 Comparitive Importance of Multi-Resolution Imagery. Proceedings of GEOBIA 2010:
662 Geographic Object-Based Image Analysis, Ghent, Belgium, 29/06–02/07/2010; 38 (4/C7), 6.
663 Wu T.F., Lin C.J., and Weng R.C., 2004. Probability estimates for multi-class classification by
664 pairwise coupling. Journal of Machine Learning Research, 5, 975-1005.
665 http://www.csie.ntu.edu.tw/~cjlin/papers/svmprob/svmprob.pdf.

Yousefi S., Tazeh M., Mirzaee S., HR Moradi H.R., Tavangar S.H., 2011. Comparison of different classification algorithms in satellite imagery to produce land use maps (Case study: Noor city). J. Appl. RS GIS Tech. Nat. Res. Sci., 2, 15-25.

Yu L., Porwal A., Holden E.-J., Dentith M. C., 2012. Towards automatic lithological classification from remote sensing data using support vector machines. Computers & Geosciences, 45, 229-239.

Zhu G., Blumberg D.G., 2002. Classification using ASTER data and SVM algorithms;: The case study of Beer Sheva, Israel, Remote Sensing of Environment, 80 (2), 233-240, ISSN 0034-4257. DOI: 10.1016/S0034-4257(01)00305-4.

Notation list	
A_L	band-specific additive rescaling factor from the metadata (radiance)
AOI	areas of interest
APW	agricultural plastic waste
A_ρ	band-specific additive rescaling factor from the metadata (reflectance)
CT	crop type
DN	digital numbers
EVA	ethylen vinyl acetate
FSO	feature space optimization
GE-1	GeoEye-1
GIS	geographical information system

GSD	ground sample distance
HDPE	high density polyethylene
L_λ	TOA spectral radiance ($Wm^{-2}srad^{-1}\mu m^{-1}$)
LDPE	low density polyethylene
M_L	Band-specific multiplicative rescaling factor from the metadata (radiance)
M_ρ	Band-specific multiplicative rescaling factor from the metadata (reflectance)
MLC	maximum likelihood classification
MTL	material library
NN	neural network
OBIA	object-based image analysis
OLI	operational land imager
PA	plastic application
PP	polypropylene
PWI	plastic waste index
Q_{cal}	quantized and calibrated standard product pixel values (DN)
RBF	radial basis function
RGB	red, green, and blue
ROI	region of interest
PVC	polyvinyl chloride
SVMs	support vector machine
SNR	signal-to-noise
TIRS	thermal infrared sensor
TM	thematic mapper
TOA	top of atmosphere

VHR	very high-resolution
WV-2	WorldView-2
θ_{SE}	local sun elevation angle (°)
θ_{SZ}	local solar zenith angle (°)
$\rho\lambda$	TOA planetary reflectance
$\rho\lambda'$	TOA planetary reflectance, without correction for solar angle

Acknowledgements

The contribution to programming and executing this research must be equally shared between the Authors.

The present research was partially carried out as a part of the project "AWARD Agricultural Waste valorisation for a competitive and sustainable Regional Development", European Territorial Cooperation Programme Greece-Italy 2007-2013, Contract n. I3.11.03.

Figure Captions

Figure 1: The study area located in Southern Italy.

Figure 2: Landsat8 OLI-TIRS image (May 19, 2013) - RGB: 432. Red box: study area.

Figure 3: Google Earth high resolution image (May 18, 2013). Red box: study area.

694 Figure 4: Land use map obtained from the Landsat8 image.

695 Figure 5: Spectral signatures of Film and Net.

696

697

698

699

700

701

702

703

704